Remote Sensing of Environment 133 (2013) 128–140

Contents lists available at SciVerse ScienceDirect

Remote Sensing of Environment

journal homepage: www.elsevier.com/locate/rse

Modelling leaf chlorophyll content in broadleaf and needle leaf canopies from ground, CASI, Landsat TM 5 and MERIS reflectance data

H. Croft [a,*], J.M. Chen [a], Y. Zhang [b], A. Simic [c]

[a] University of Toronto, Department of Geography, Toronto, Canada M5S 3G3
[b] Delta State University, Division of Biological and Physical Sciences, Cleveland, MS 38733, USA
[c] University of Victoria, Department of Geography, Victoria, British Columbia, Canada V8P 5C2

ARTICLE INFO

Article history:
Received 19 August 2012
Received in revised form 28 January 2013
Accepted 3 February 2013
Available online 15 March 2013

Keywords:
Chlorophyll content
LAI
PROSPECT
Canopy structure
Broadleaf
Needle leaf

ABSTRACT

Foliar chlorophyll content in forested ecosystems plays a fundamental role in plant photosynthesis and can indicate vegetation stress and disturbance. However, leaf chlorophyll retrieval is complicated as canopy reflectance in the visible and near-infrared wavelengths is affected by confounding effects not only from leaf pigment concentration but also leaf area index (LAI), canopy architecture, illumination and viewing geometry and understory vegetation. Unlike empirical indices, which are often developed at leaf-level and can be species, site and time specific, a process modelling approach can account for the variation of other variables affecting canopy reflectance; therefore providing a more accurate estimate of chlorophyll content over multiple vegetation species, time-frames and across broader spatial extents. This study used a linked canopy (4-Scale) and leaf (PROSPECT) modelling approach to investigate the ability of radiative transfer models to estimate foliar chemistry for different vegetation types (broadleaf and needle leaf) from optical remote sensing data. Coniferous and deciduous sites were selected in Ontario, Canada, representing different dominant vegetation species, including black spruce (*Picea mariana*), sugar maple (*Acer saccharum*) and trembling aspen (*Populus tremuloides*), and a variety of canopy closures and structures. These sites were sampled over multiple time-frames to collect ground data including leaf area index, leaf reflectance spectra (400–2500 nm) and laboratory leaf chlorophyll content. Canopy reflectance data were acquired from the Compact Airborne Spectrographic Imager (CASI), Landsat 5 TM and Medium Resolution Imaging Spectrometer (MERIS). The model results show that leaf chlorophyll content derived from satellite images demonstrates a good relationship with measured leaf chlorophyll content, with validation results of $R^2 = 0.62$; $p<0.001$ (MERIS) and $R^2 = 0.65$; $p<0.001$ (Landsat 5 TM), and a strong linearity with negligible systematic bias. CASI data gave a regression coefficient of $R^2 = 0.41$ ($p<0.05$) on a reduced dataset. This research provides theoretical and operational bases for the future retrieval of leaf chlorophyll content across different vegetation species, canopy structures and over broad spatial extents; crucial characteristics for inclusion in photosynthesis and carbon cycle models.

1. Introduction

Foliar pigments such as chlorophyll *a* and *b* play a crucial role in plant photosynthesis through the conversion of solar radiation into stored chemical energy and can provide important information on gross primary productivity (Curran et al., 1990; Gitelson et al., 2006). The amount of solar radiation absorbed by a leaf is largely a function of foliar concentrations of photosynthetic pigments, therefore low concentrations of chlorophyll can directly limit photosynthetic potential and hence primary production (Richardson et al., 2002). Chlorophyll distribution in vegetation is also strongly related to leaf nitrogen content (Daughtry et al., 2000) and highlights areas of plant disturbance and stress, thus acting as a bio-indicator of plant physiological condition (Gitelson et al., 2003; Sampson et al., 2003; Zarco-Tejada et al., 2002). Research shows that chlorophyll content declines more rapidly than carotenoid content when plants are experiencing stress or during leaf senescence (Merzlyak & Gitelson, 1995; Sims & Gamon, 2002), resulting in changes in green peak reflectance (~550 nm) and along the red edge (690 to 750 nm) (Zarco-Tejada et al., 2001). Physiologically, the variation in leaf chlorophyll between and within species and how it responds to changing biotic and abiotic factors is of ecological importance (Richardson et al., 2002). Chlorophyll content is also linked to carbon and nitrogen cycles and its role in photosynthesis and net primary productivity is important within regional and global carbon models (Inoue, 2003). The accurate monitoring of canopy chlorophyll content across a range of temporal and spatial scales is therefore paramount for monitoring and understanding a number of ecosystem responses.

In order to accurately model variations in leaf biochemical properties over large spatial extents and at fine temporal scales, a remote

* Corresponding author. Tel.: +1 4169783375.
E-mail address: holly.croft@utoronto.ca (H. Croft).

0034-4257/$ – see front matter © 2013 Elsevier Inc. All rights reserved.
http://dx.doi.org/10.1016/j.rse.2013.02.006

sensing approach is essential. There has been considerable research devoted to investigating leaf optical properties, through the derivation of statistical relationships with biochemical constituents, in order to retrieve chlorophyll content (le Maire et al., 2004; Sims & Gamon, 2002). At the leaf level, reflectance is controlled by the presence of foliar constituents such as chlorophyll, carotenoids, and water (Asner & Martin, 2008; Ustin et al., 2004). Whilst many empirical indices show strong relationships with chlorophyll content, they have often been developed and tested using a few closely related species, at the leaf scale and under controlled laboratory conditions (Blackburn, 1998; Gamon & Surfus, 1999; Gitelson et al., 2003; le Maire et al., 2004). When scaling up from a leaf to a branch or canopy, and in field conditions, additional variables affect the measured reflectance signal. At the canopy level, reflectance is also governed by leaf architecture, leaf area index (LAI), clumping, canopy height, density, non-photosynthetic canopy elements (Demarez & Gastellu-Etchegorry, 2000; Simic et al., 2011), along with solar/viewing geometry, ground cover and understory vegetation (Broge & Leblanc, 2001). It is therefore possible that reflectance factors from two forest canopies may be different even if the reflectance spectra of the constituent leaves are the same (Blackburn, 1998). Consequently, applying empirical indices over larger spatial extents is problematic and often results in weaker relationships with ground data (Jacquemoud et al., 2000).

In order to relate leaf biophysical processes to reflectance factors at the forest stand scale, a physically based modelling approach is needed to account for variations in canopy architecture, image acquisition conditions and background vegetation. Research has demonstrated the potential of using linked canopy and leaf radiative transfer models for deriving leaf biochemical constituents (Demarez & Gastellu-Etchegorry, 2000; Moorthy et al., 2008; Simic et al., 2011; Zarco-Tejada et al., 2001; Zhang, 2011; Zhang et al., 2008a). However, previous studies have often focused on one vegetation type (and leaf and canopy structure) and used reflectance data collected from airborne platforms. It is crucial therefore, to assess the accuracy of such modelling approaches across different vegetation species and across open and closed canopies. A key question is how well variations in leaf and canopy structure can be accounted for in efforts to model leaf chlorophyll content over broader spatial extents and multiple time-frames.

This study assesses the potential for deriving leaf chlorophyll using a modelling approach from satellite-derived data, in order to estimate leaf chlorophyll content over regional spatial extents and finer temporal scales, afforded by the higher temporal revisit capabilities of satellite mounted sensors. In particular, the MEdium Resolution Imaging Spectrometer (MERIS) was selected due to its very short revisit time (2–3 days), narrow-band wavelengths covering wavelengths applicable to vegetation studies (15 bands ranging from 390 nm to 1040 nm) and its high radiometric accuracy (Curran & Steele, 2005). However, the coarse spatial resolution (MERIS; 1200 m) of such satellite measurements render ground validation difficult, often resulting in a weak relationship between ground- and satellite-based observations, in part due to spatial heterogeneity in vegetation properties that can exist with a coarse pixel (>1 km) (Fisher & Mustard, 2007; Jenkins et al., 2002). Consequently, an intermediary and independent source of data is needed to understand the implications of spatial scale on variable measurement and validate the algorithm at multiple spatial scales (Chen et al., 2002; Fisher & Mustard, 2007).

In this paper, we detail a methodology for deriving leaf chlorophyll content from satellite observations, compare leaf chlorophyll estimates derived from airborne and two independent satellite sensors, and validate the estimates against ground measurements from two study sites in Ontario, Canada. The objectives of this research are to:

- evaluate the retrieval of leaf chlorophyll content from MERIS satellite data using a physical modelling approach;
- validate modelled leaf chlorophyll estimates using an independent satellite data source and measured ground data;
- investigate the impacts of spatial resolution and spatial scale on leaf chlorophyll estimates.

2. Methods

2.1. Field sites and ground data collection

2.1.1. Haliburton forest

Field sampling was conducted out in a mature sugar maple (*Acer saccharum* M.) stand located in Haliburton Forest, Ontario, Canada (45° 14′ 15.5″N, 78° 32′ 18.0″ W; Fig. 1). Haliburton forest falls within the Great-Lakes–St.-Lawrence region (Rowe, 1972), with an average annual precipitation of approximately 1050 mm and mean annual temperature of 5 °C (Gradowski & Thomas, 2006). The site is underlain by shallow brunisols or juvenile podzols (pH 4.2–5.1); mainly silty sands from Precambrian Shield granite or granite-gneiss deposits (Gradowski & Thomas, 2006). The upland hardwood forests of Haliburton Forest are dominated by sugar maple but also contain beech (*Fagus grandifolia* Ehrh.), eastern hemlock (*Tsuga canadensis* (L.) Carr.), and yellow birch (*Betula alleghaniensis* Britt.) (Caspersen & Saprunoff, 2005). Ground-based sampling in the sugar maple (SM) stand was carried out 7 times during 2004 growing season from 10th June to 30th September (Zhang et al., 2007).

2.1.2. Sudbury

A total of eleven sites were sampled located northwest of Sudbury, Ontario (46° 49′ 13″ N to 47° 12′ 9″ N and 81° 22′ 2″ W to 81° 54′ 30″ W; Fig. 1). The sites are situated at an elevation of approximately 350 m above sea level, with a flat topography and underlain by shallow soils on Canadian Shield bedrock. Temperatures range from −40 °C to 30 °C, with a mean annual temperature of 5 °C and mean annual precipitation of approximately 800 mm (Leithead et al., 2012), with snow-covered ground from December to March (Rayfield et al., 2005). The dominant vegetation includes black spruce (*Picea mariana* Mill.) and jack pine (*Pinus banksiana*), with deciduous forest patches containing aspen (*Populus tremuloides* Michx). Six black spruce (BS) sites were sampled in the summer of 2003 and 2004 (Zhang et al., 2008a), and three black spruce and two trembling aspen (As) sites during the summer of 2007 (Simic et al., 2011). The sites contain mature black spruce stands of different ages and crown closures. Understory species included bog Labrador tea (*Ledum groenlandicum* Oeder), lichen (*Cladonia cristatella*), Feathery Bog-moss (*Sphagnum cuspidatum*), grass and bog rosemary (*Andromeda polifolia*) and dense green moss (Zhang et al., 2008a).

The selected deciduous and coniferous sites represent a range of canopy structural conditions (LAI and foliage clumping index (Ω)), leaf types and vegetation health (Table 1).

2.1.3. Leaf reflectance and chlorophyll content

Leaf reflectance factors and chlorophyll content (μg/cm^2) were measured in order to validate modelled results from airborne and satellite-derived data. Leaves and shoots were sampled from the upper canopy using a shotgun, sealed in plastic bags and kept at a temperature of 0 °C for further analysis (Zhang et al., 2007). Leaf reflectance and transmittance were measured with an ASD spectroradiometer Fieldspec Pro FR (Analytical Spectral Devices, Inc. Boulder, USA) attached via a fiber optic cable to a Li-Cor 1800 integrating sphere (Li-Cor 1800-12S, Li-COR, Inc., Lincoln, Nebraska, USA). Reflectance and transmittance spectra were measured using methods described by Harron (2000). The needle leaves were placed in specially designed black anodized carriers to take spectral measurements (Harron & Miller, 1995; Zhang et al., 2008b). For broadleaf samples, leaves were clamped into the sample port on the sphere wall (Zhang et al., 2007). Total leaf chlorophyll

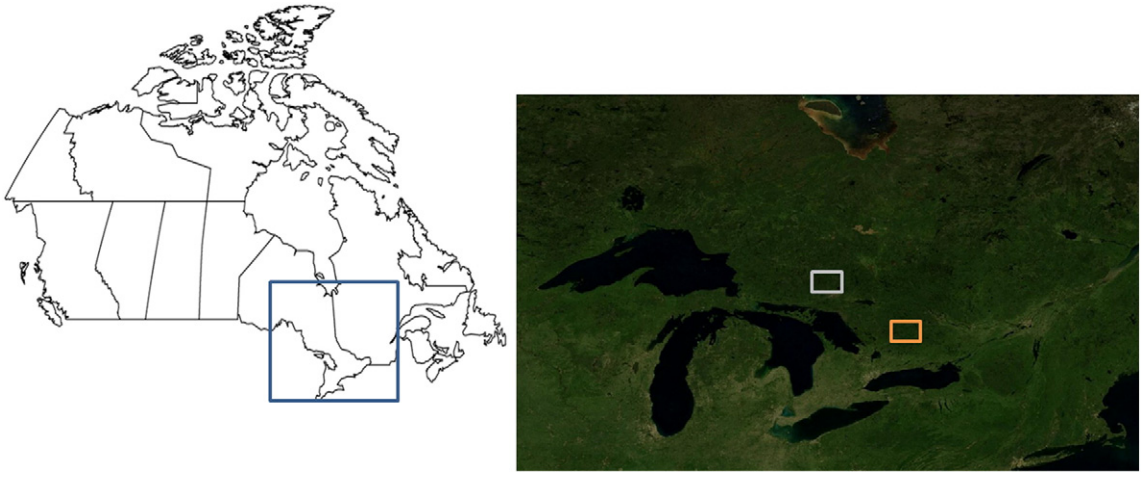

Fig. 1. Site locations of Haliburton (orange outline) and Sudbury (grey outline) in Ontario, Canada.

(Chl a + b) content (μg/cm^2) was measured using the method reported by Moorthy et al. (2008).

2.1.4. Canopy structural parameters

Leaf area index and forest canopy structure are important parameters in retrieving leaf-level reflectance factors from airborne and satellite platforms using canopy reflectance models. Canopy architecture can also play a perturbing role in modelling leaf chlorophyll content from reflectance factors (Blackburn, 1998). Consequently, it is important to obtain accurate ground measurements of forest structural parameters in order to validate satellite-derived measurements of LAI. Effective LAI (*Le*) was measured using the LAI-2000 plant canopy analyser (Li-Cor, Lincoln, NE, USA) (Chen et al., 1997). The element clumping index and leaf area index were measured using TRAC (Tracing Radiation and Architecture of Canopies) (Chen & Cihlar, 1995). Structural parameters of trees (density, height and diameter breast height) were also measured and understory reflectance was measuring using the ASD Fieldspec Pro Spectroradiometer for the dominant species present at each site (Simic et al., 2011; Zhang et al., 2008a).

2.2. Remote sensing data acquisition and processing

2.2.1. Airborne CASI data

Hyperspectral airborne images were acquired by the Compact Airborne Spectrographic Imager (CASI) over five black spruce sites on September 5, 2003 and all six sites from 14–16th August, 2004 (Table 2). CASI records on-nadir radiance in 72 channels at a 7.5 nm spectral resolution from 408 nm to 947 nm at a 2 m spatial resolution. The images were radiometrically corrected to "at sensor" radiance by the Earth Observations Laboratory at York University and atmospherically corrected using CAM5S and ground aerosol optical depth to give reflectance data (O' Neill et al., 1997). The CASI imagery was georeferenced using GPS data and visual identification of 2×2 m ground white targets collected at the centre of the sites, Final reflectance spectra were generated after flat field adjustments were applied (Zhang et al., 2008a). The CASI data were spatially aggregated to Landsat scale (30 m) spatial resolution to allow direct comparison in differences in Landsat and CASI spectral resolution on chlorophyll retrieval and due to the modelling characteristics of the 4-Scale canopy model (Section 2.3.1), where reflectance inputs must contain a number of tree crowns within a pixel.

2.2.2. Satellite Landsat 5 TM data

In order to assess how modelled foliar chlorophyll content changes across different spatial sampling units, from ground-based leaf-level measurements to medium spatial resolution satellite data (1200 m), an intermediary satellite data source from Landsat 5 TM (30 m) was employed. The Landsat 5 TM images were radiometrically and geometrically corrected and georeferenced to UTM map projection. Landsat scenes were selected as closely as possible to the time frame of ground

Table 1
Site locations, structural parameters and vegetation type and condition.

Location	Site ID	Location	Vegetation	LAI	ΩE	Condition
Haliburton	Ha164	45°14′16″N, 78°32′18″W	Broadleaf	4.12	0.86	Healthy
	Ha193	45°14′16″N, 78°32′18″W	Broadleaf	7.15	0.90	Healthy
	Ha199	45°14′16″N, 78°32′18″W	Broadleaf	–	–	Healthy
	Ha214	45°14′16″N, 78°32′18″W	Broadleaf	5.45	0.98	Healthy
	Ha246	45°14′16″N, 78°32′18″W	Broadleaf	–	–	Healthy
	Ha263	45°14′16″N, 78°32′18″W	Broadleaf	5.34	0.94	Healthy
	Ha275	45°14′16″N, 78°32′18″W	Broadleaf	4.86	0.93	Healthy
Sudbury 2003 and 2004	Sb2	47°12′08″N, 81°54′29″W	Needle leaf	3.97	0.81	Healthy
	Sb3	46°49′17″N, 81°22′06″W	Needle leaf	2.36	0.88	Stressed
	Sb4	46°49′13″N, 81°22′30″W	Needle leaf	3.21	0.84	Stressed
	Sb5	46°54′27″N, 81°25′11″W	Needle leaf	3.09	0.80	Healthy
	Sb7	47°09′45″N, 81°44′32″W	Needle leaf	1.14	0.85	Stressed
	Sb9	47°11′58″N, 81°52′01″W	Needle leaf	3.83	0.84	Healthy
Sudbury 2007	As25	47°09′48″N, 81°42′23″W	Broadleaf	4.16	0.86	–
	As26	47°09′32″N, 81°43′09″W	Broadleaf	2.23	0.85	–
	Sb17	47°09′50″N, 81°44′36″W	Needle leaf	4.99	0.81	–
	Sb24	47°10′19″N, 81°42′33″W	Needle leaf	3.94	0.87	–
	Sb8	47°09′45″N, 81°43′37″W	Needle leaf	2.58	0.84	Stressed

Table 2
Ground, CASI, Landsat 5 TM and MERIS data acquisition dates and conditions.

Location	ID	Ground	CASI		Landsat 5 TM		MERIS	
		Date	Date	ϑ_i, ϑ_r, φ	Date	ϑ_i, ϑ_r, φ	Date	ϑ_i, ϑ_r, φ
Haliburton	Ha162	10/06/04	–	–	04/06/04	30°,0°,134°	25/06/04	31°,29°,25°
	Ha183	01/07/04	–	–	06/07/04	30°,0°,130°	17/07/04	32°,17°,65°
	Ha209	27/07/04	–	–	–	–	01/08/04	31°,25°,143°
	Ha229	16/08/04	–	–	16/08/04	37°,0°,139°	24/08/04	40°,9°,39°
	Ha243	30/08/04	–	–	–	–	02/09/04	41°,17°,135°
	Ha255	11/09/04	–	–	–	–	19/09/04	49°,33°,45°
	Ha274	30/09/04	–	–	–	–	05/10/04	55°,17°,49°
Sudbury	2003	08/03	05/09/03	40°,0°,0°	16/06/03	30°,0°,133°	14/08/03	35°,19°,140°
Sudbury	2004	08/04	14–16/08/04	30–55°,0°,0°	11/06/04	30°,0°,136°	07/08/04	38°,6°, 38°
					05/08/04	35°,0°,140°		
Sudbury	2007	08/07	–	–	11/06/07	29°,0,°141°	13/08/07	36°,15°,140°

ϑ_i = *solar zenith angle;* ϑ_r = *viewing zenith angle;* φ = *azimuth angle.*

data collection (Table 2). The Landsat scenes were atmospherically corrected using cosine estimation of atmospheric transmittance (COST model; Chavez, 1996). Whilst radiative transfer methods (e.g. 6S and MODTRAN (Berk et al., 1998; Vermote et al., 1997)) can produce more accurate results, they usually require coincident atmospheric measurements such as aerosol optical depth, water vapour and ozone, to parameterise the model (Sharma et al., 2009). Mahiny and Turner (2007) found that 6S produced anomalous results when all the detailed data on atmospheric condition that is required was not used. As these measurements were not available, this study used the COST model (Chavez, 1996), which is an absolute image-based method (Mahiny & Turner, 2007). In the COST model, the cosine of sun zenith angle is used to approximate the effects of absorption by atmospheric gases and Rayleigh scattering for individual spectral bands (Eq. (1)).

$$\rho = \pi * d^2 * (L_{\lambda sat} - L_{\lambda haze}) / \mathrm{ESUN}_\lambda * \cos^2\theta \quad (1)$$

where p = reflectance factor; $L_{\lambda sat}$ = spectral radiance at the sensor; $L_{\lambda haze}$ = path radiance; d = earth–sun distance (AU); ESUN = mean solar exoatmospheric irradiances; solar zenith angle (°). The solar exoatmospheric spectral irradiances (ESUN) for the Landsat 5 TM were obtained from Chander et al. (2009), based on previous calculations from Markham and Barker (1986). Path radiance ($L_{\lambda haze}$) was obtained from pixels of known zero reflectance like large deep waterbodies and assuming that any value in the raw image in these areas other than zero represents haze effects. This value was subsequently verified through a band specific histogram analysis by examining the step in pixel radiance values, usually occurring at 1% for the image (Chavez, 1988).

2.2.3. Satellite MERIS data

Ten MERIS Reduced Resolution Level 2 (1200 m) images were used, covering both Haliburton and Sudbury study sites (Table 2). MERIS is a medium-spectral resolution imaging spectrometer, measuring surface reflectance in fifteen spectral bands from 415–885 nm and has a temporal revisit time of 2–3 days. MERIS Level 2 (L2) products are radiometrically and atmospherically corrected, for Rayleigh scattering, ozone, water vapor absorption and aerosol content. The Level 2 products contain both surface reflectance and geolocated geophysical parameters, including geometric information, solar and viewing geometry, terrain height, some meteorological data and several flags that address the quality and the validity of the image (Canisius et al., 2010). The MERIS Level 2 images were reprojected to WGS 84 and UTM coordinate system (UTM 18) and resampled using nearest neighbour interpolation using the BEAM VISAT software application. The MERIS images were also co-registered and geometrically corrected using tie points, which were distributed evenly throughout the image and contained geo-location coordinates.

2.2.4. Landsat and MERIS spectral comparison

Sensors on different satellite platforms can measure spectral radiance across a range of different wavebands and bandwidths, with systematic differences occurring according to different measured components of surface variables within a pixel (Guyot & Gu, 1994; Steven et al., 2003). It is therefore not possible to directly compare reflectance factors from sensors sampled at differing bandwidths. In order to use Landsat data for this study, differences in reflectance that arose from sensor characteristics was explored in order to derive an adjustment factor for comparability with MERIS data. Landsat 5 bands were simulated from hyperspectral reflectance from a typical black spruce reflectance spectra, sampled using an ASD spectroradiometer (Section 2.1.3). The spectral response function of a sensor describes its relative sensitivity to different wavelengths, and was used to calculate reflectance factors in simulated Landsat bands, as a weighted sum of hyperspectral reflectance and the SRF (Eq. (2)).

$$L = \sum_{\lambda=1}^{N} \beta(\lambda) L'(\lambda) / \sum_{\lambda=1}^{N} \beta(\lambda) \quad (2)$$

where L and $L'(\lambda)$ is reflectance in the larger bandwidth and reflectance data in the original wavelength and $\beta(\lambda)$ is the weight of the spectral response function (Chen et al., 2002). Simulated bands have also been used to investigate the effects of different sensor bandwidths and spectral response functions on NDVI values, and to formulate corrections for biases to allow cross sensor comparisons (Steven et al., 2003). Fig. 2 demonstrates the differences in reflectance that occurs as a result of broader bandwidths (simulated from hyperspectral reflectance) for a typical black spruce reflectance spectra, compared to hyperspectral and simulated MERIS data.

Fig. 2 shows that the greatest differences between MERIS and Landsat-derived reflectance occurs in green and red wavelengths, where there are larger variations in hyperspectral reflectance factor across the Landsat band extent. The sub-band variations in reflectance are 'smoothed' by the larger Landsat bandwidth, causing simulated Landsat reflectance factors in the green band (520–600 nm) for example, to be >10% lower than then the simulated MERIS-derived reflectance at 560 nm (±10 nm). Consequently, correction factors were derived for both broadleaf and deciduous species, to empirically correct Landsat reflectance to MERIS narrowband reflectance, and to compensate for this spectral smoothing across larger bandwidths. The correction factors are shown in Fig. 2 for the MERIS bands which spectrally overlap with Landsat bands, with two additional MERIS bands at 445 nm and 755 nm, due to their spectral proximity to the Landsat bands (<5 nm) in a region showing negligible spectral changes between the hyperspectral data and Landsat data. The correction factors were calculated using hyperspectral leaf reflectance rather than canopy reflectance, which may be contribute to some

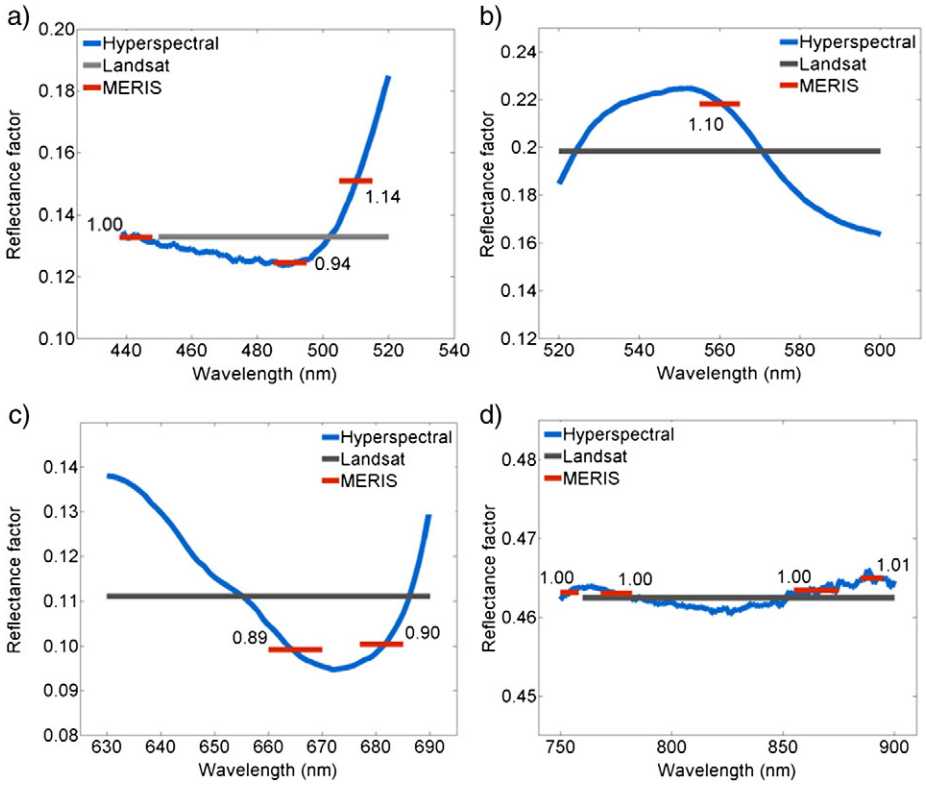

Fig. 2. Differences in needle leaf reflectance according to spectral bandwidth for hyperspectral data and simulated Landsat and MERIS reflectance, shown for Landsat bands a) blue; b) green; c) red; d) NIR. The values represent the correction factors for Landsat derived reflectance to MERIS bands.

uncertainty in corrected results for the canopy data, particularly in the NIR, due to the presence of additional canopy variables and background contributions. As the 620 nm MERIS band was not covered by Landsat data, it was modelled by linear spectral interpolation between the 560 nm and 665 nm bands, in accordance with the linearity between 560–620 nm for MERIS derived reflectance factors. This interpolation was considered important in order to compare the modelled chlorophyll content from Landsat and MERIS sensors as a result of differences in spatial scale rather than as a result of differences in the spectral input into PROSPECT. Whilst the interpolation in canopy reflectance data was linear, the algorithm to model leaf reflectance from canopy reflectance is wavelength dependent and will lead to reflectance factors at 620 nm independent of reflectance at 560 and 665 nm. In order to assess the error associated with modelling chlorophyll from reduced wavebands and coarser bandwidths relative to hyperspectral reflectance, the PROSPECT leaf radiative transfer model was used to compare derived chlorophyll values (see Section 2.3 for more details). The RMSE values from MERIS, Landsat and 'Landsat adjusted' chlorophyll estimates against hyperspectral derived chlorophyll were found to be 0.67, 1.60 and 0.91 ug/cm^2, respectively. The chlorophyll estimates using original Landsat bands also demonstrate a strong performance in chlorophyll retrieval, although the Landsat adjustment further reduces the error in modelled chlorophyll by 0.59 ug/cm^2.

2.3. Modelling leaf chlorophyll content

Foliar chlorophyll content was modelled using a canopy geometrical–optical model (4-Scale; Chen & Leblanc, 1997) linked with a leaf radiative transfer model (PROSPECT; Jacquemoud & Baret, 1990). The linking of canopy and leaf models to retrieve leaf and canopy chlorophyll content has been demonstrated previously using a range of different model combinations, mainly using airborne data. These include SAILH (Kuusk, 1985) with LIBERTY (Dawson et al., 1998) and PROSPECT (Moorthy et al., 2008), SPRINT (Goel & Thompson, 2000) and PROSPECT (Zarco-Tejada et al., 2004) and 4-Scale with PROSPECT for airborne CASI data (Simic et al., 2011; Zhang et al., 2007, 2008a).

2.3.1. Leaf reflectance inversion

For canopy modelling, whilst many studies have previously used turbid medium models such as SAIL (Verhoef, 1984), these models do not take account of canopy structural variables, such as crown shape, clumping of foliage elements and tree distribution. Crown shadowing dominates in closed canopies and the effects of background reflectance and shadows dominate in open canopies (Chen & Leblanc, 1997; Demarez & Gastellu-Etchegorry, 2000). As forest canopies cannot be treated simply as a turbid medium, the integration of geometrical-optical techniques can be used to correct for the influences of canopy architecture on reflectance factors and account for multiple scattering effects (Chen & Leblanc, 1997; Gastellu-Etchegorry et al., 1996; Li et al., 1995). This is because reflected radiance from shaded components is determined by first-order scattering (separating sunlit and shaded components), and then multiple scattering from subsequent interactions between light and vegetation or background material (Chen & Leblanc, 2001). Crucially for this study, hybrid models apply the scientific principles of both geometric and turbid medium models, and can therefore be applied to both sparse and dense canopies (Goodenough et al., 2006). The 4-Scale model (Chen & Leblanc, 1997) simulates the bi-directional reflectance distribution function (BRDF) based on canopy architecture at four scales: 1) tree groups, 2) tree crown geometry, 3) branches, and 4) foliage elements (Chen & Leblanc, 2001). The model considers both the structural effects of tree branches and scattering elements and also the spatial distribution of tree groups and the geometry of tree crowns. Deciduous crowns are modelled as a spheroid and coniferous crowns as a cone and cylinder, both of variable dimensions. A crown is represented as a complex medium, where mutual shadowing

occurs between shoots or leaves, meaning that sunlit foliage can be viewed on the shaded side and shadowed foliage can be viewed on the sunlit side.

4-Scale was run in the forward mode, using fixed and variable structural parameters and leaf and understory reflectance spectra to model canopy reflectance. To derive leaf level reflectance, the 4-Scale model was inverted using a look-up-Table (LUT) approach. LUT methods are computationally efficient and can overcome the difficulty of local minima, by giving the global minimum, providing the variable space is sufficiently sampled (Jacquemoud et al., 2009). The fixed structural parameters were based on ground measurements and reported values in the literature (e.g. Chen & Leblanc, 1997) and are listed in Table 3. Zhang et al. (2008a) provide a discussion of the sensitivity of the model to certain canopy structural parameters, including LAI, stem density, tree height and crown radius. Variable parameters were solar zenith angle (ϑ_i), viewing zenith angle (ϑ_r), and azimuth angle (φ) which were obtained from image acquisition metadata, and LAI which was calculated using an empirical algorithm (discussed further in Section 2.3.3).

The element clumping index (Ω_E) is related to canopy architecture and properties such as crown size and tree density (Kurcharik et al., 1997) and is important for estimating radiation interception and distribution in plant canopies (Simic et al., 2010). The non-random spatial distribution of trees is simulated using the Neyman type A distribution (Chen & Leblanc, 1997); representing clumping and patchiness within a forest stand. Fr controls the repulsion effect which determines if branches from one tree are allowed to overlap with branches from other trees. Fr = 1 means maximum repulsion and no overlap at nadir and Fr = 0 means no repulsion and overlapping is allowed. In addition to the canopy variables listed in Table 3, the composition and reflectance properties of the forest floor also affect the accuracy of modelled chlorophyll content values (Verrelst et al., 2010; Zarco-Tejada et al., 2004; Zhang et al., 2008a). An understory layer was therefore included to represent the optical properties of background components at both the Haliburton and Sudbury test sites.

Based on the input parameters, the 4-Scale model calculates canopy reflectance as a linear summation of four components (Chen & Leblanc, 2001); the sunlit vegetation (ρ_{PT}), shaded vegetation (ρ_{ZT}), sunlit ground (ρ_{PG}) and shaded ground (ρ_{ZG}), as shown in Eq. (3), where F_{PT}, F_{PG}, F_{PG} and F_{ZT} represent the probability of viewing each component, respectively.

$$\rho = \rho_{PT}F_{PT} + \rho_{ZT}F_{ZT} + \rho_{PG}F_{PG} + \rho_{ZG}F_{ZG} \quad (3)$$

4-Scale also includes a multiple scattering scheme for 2nd order scattering and above (Chen & Leblanc, 2001). In order to derive leaf reflectance from canopy reflectance, the enhancement of both sunlit and shaded reflectance due to multiple scattering must be accounted for, using a multiple scattering factor (M factor; Simic et al., 2011; Zhang et al., 2008a). This was calculated using the proportions of sunlit and shaded components output from 4-Scale:

$$M = \frac{\rho - \rho_{PG}F_{PG}}{\rho_L F_{PT}} \quad (4)$$

where ρ is the canopy-level reflectance simulated by 4-Scale, ρ_L is measured leaf reflectance, ρ_{PG} is background reflectance and F_{PG} is the fraction of background reflectance. Finally, the M factor (Eq. (4)) is used to invert satellite reflectance data to model leaf reflectance factor (ρ_L).

$$\rho_L = \frac{\rho_{satellite} - \rho_{PG}F_{PG}}{MF_{PT}} \quad (5)$$

The use of the M factor allows for the simplification of Eq. (3) into Eq. (5), and it serves for two purposes: (1) to include the two less variable shaded components, and (2) to convert the sunlit crown reflectance to sunlit leaf reflectance. The LUT developed using the 4-Scale model includes the variations of the two shaded components with sun and view angles and canopy geometry.

2.3.2. Leaf chlorophyll content retrieval

The leaf radiative transfer model PROSPECT (Jacquemoud & Baret, 1990) was selected to generate leaf chlorophyll content based on the modelled leaf reflectance spectra. Leaf optical properties (reflectance and transmittance) from 400 to 2500 nm are defined in PROSPECT as a function of four parameters: structure parameter, chlorophyll (a + b) concentration, dry matter content and water. Absorption is calculated as the linear summation of the specific absorption coefficients of biochemical constituents and their respective concentrations. PROSPECT has had widespread validation across a number of vegetation species and functional types, including broadleaf (Demarez & Gastellu-Etchegorry, 2000; Jacquemoud et al., 1995a,b) and coniferous trees (Kötz et al., 2004; Zarco-Tejada et al., 2004). It also requires a smaller number of input parameters than other leaf-level models, is readily inverted (Moorthy et al., 2008) and there is good agreement between reflectance spectra and chlorophyll content in forward simulations (Zarco-Tejada et al., 2004). Due to the inclusion of both broadleaves and conifer needles in the study sites, a version of PROSPECT modified for application with conifer needles (Zhang et al., 2008b) was used, which introduced a leaf thickness factor to account for the effects of changes in the leaf width relative to leaf thickness on light absorption (Zhang et al., 2008b). Modelled leaf transmittance was derived from the spectral ratio of measured reflectance and transmittance for broadleaf and needle leaf samples and applied to modelled leaf reflectance, derived from Eq. (5) (Zhang et al., 2008a).

2.3.3. Leaf area index

LAI is a highly spatially and temporally variable structural parameter influencing the probabilities of viewing the sunlit foliage and background and the multiple scattering factor (Simic et al., 2010; Zhang et al., 2008a). Due to its variation in space and time, LAI was also derived from the CASI, Landsat and MERIS satellite imagery to give spatially-continuous LAI values. Satellite imagery has demonstrated results for LAI retrieval at a range of different spatial and temporal scales (Abuelgasim et al., 2006; Chen & Cihlar, 1996; Chen et al., 2002; Weiss et al., 2007). The Reduced Simple Ratio (RSR) has shown a more linear relationship with LAI than NDVI and is less likely to saturate at higher LAI conditions (Chen et al., 2002). In comparison to the simple ratio (SR; Red/NIR), RSR (Eq. (6)) is less sensitive to differences in cover types, enabling more accurate modelling of LAI in mixed cover types and allowing the development of a single LAI algorithm (Chen et al., 2002). RSR is also less influenced by background

Table 3
Canopy structural parameters and background component for coniferous and vegetation sites.

Parameter	Deciduous	Coniferous
Stick height (Ha)	10 m	5 m
Crown height (Hb)	8 m	5 m
Crown radius (R)	1.25 m	0.85 m
Crown shape	Spherical	Cone + cylinder
Tree density (per hectare)	1100	2800
Neyman tree grouping factor	2	4
Element clumping index (ΩE)	0.8	0.89
Needle:shoot ratio (γE)	1	1.4
Element width (Ws)	0.15 m	0.04 m
Repulsion factor (Fr)	0.5	0.5
Understory vegetation	Maple saplings and wood	Soil and moss

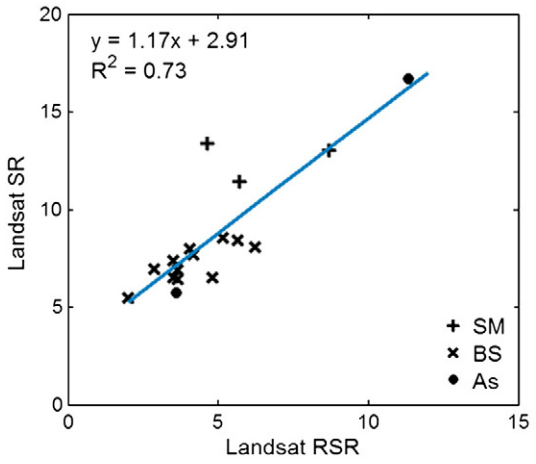

Fig. 3. Relationship between Landsat SR and Landsat RSR.

contributions (soil, moss cover, understory, leaf litter) than SR (Chen et al., 2002).

$$RSR = \frac{\rho_{NIR}}{\rho_{\rho}}\left(1-\frac{\rho_{SWIR}-\rho_{SWIR_{min}}}{\rho_{SWIR_{max}}-\rho_{SWIR_{min}}}\right) \quad (6)$$

where ρ_{NIR}, ρ_{red}, and ρ_{SWIR} are the reflectance in NIR, red, and SWIR band, respectively. Minimum and maximum SWIR reflectance ($\rho_{SWIRmin}$ and $\rho_{SWIRmax}$) were defined as the 1% minimum and maximum cut-off in SWIR reflectance histograms for each image. LAI values were modelled using empirical algorithms developed by Chen et al. (2002) in a comprehensive study of different land covers across Canada. In this paper, the Coniferous algorithm (Eq. (7)) gave the strongest results for both coniferous and deciduous species.

$$LAI = RSR/1.242 \quad (7)$$

The absence of a SWIR band in CASI and MERIS data meant that RSR could not be calculated directly for these products. Consequently, LAI values were retrieved by first correcting SR to RSR using a calibration factor derived from the relationship between Landsat SR and Landsat RSR (Fig. 3).

The modelled LAI values from RSR are shown in Fig. 4 for each data source. The CASI and Landsat LAI data were calculated as an average value from 3×3 Landsat pixels centred on the ground site to reduce positional inaccuracy and the MERIS data are shown for a 1200 m pixel.

2.3.4. Leaf chlorophyll scaled from fine- to coarse spatial resolution products

The coarse spatial scale of satellite-derived biophysical products (e.g. ≥500 m) makes validation with ground data complex and prone to uncertainty (Chen et al., 2002; Fisher & Mustard, 2007; Jenkins et al., 2002). Relationships between ground measurements and coarse scale satellite measurements may be low due to the spatial heterogeneity present within a pixel (Fisher & Mustard, 2007), not only in leaf chlorophyll content but also variables such as tree species, tree density, LAI and areas of bare ground. In this study, we used both airborne CASI and Landsat 5 TM data (30 m) to act as an intermediary between ground measurements and MERIS RR data (1200 m). The use of CASI data also allowed assessment of the impact of the coarse spectral resolution of Landsat TM data on chlorophyll estimates. Hyperspectral CASI data (aggregated to 30 m) was used to investigate the relationship between hyperspectral and broadband derived chlorophyll at a smaller number of sites due to CASI data availability; reducing the range of data available for analysis. The narrow CASI swath extent restricted the ability to also scale up CASI chlorophyll estimates to MERIS spatial resolutions.

The spatial aggregation process of reflectance factors can cause errors in coarser resolution surface parameter and algorithms that define the relationship between aggregated reflectance and the surface parameter (Simic et al., 2004). Mathematically, the correct way to obtain chlorophyll content for a coarse pixel (MERIS 1200 m), consisting of n small pixels (Landsat TM 30 m), is to calculate the chlorophyll value of each small pixel, and then take the arithmetic mean of all of the small pixels (Chen, 1999). These values and algorithms are called distributed products (Chl_D). Remote sensing products generated at coarse resolutions or where fine-scale reflectance is first aggregated to the coarse scale pixel are denoted as lumped products (Chl_L) and algorithms (Chen, 1999; Hu & Islam, 1997; Simic et al., 2004). Following the procedures outlined in Chen et al. (2002), leaf chlorophyll maps were produced for each Landsat scene using the algorithms outlined in previous sections and the same as applied to MERIS data. The fine spatial resolution chlorophyll maps were then resampled into coarse resolution (1200 m) MERIS pixels (Chl_D and Chl_L).

3. Results and discussion

3.1. Modelled leaf reflectance

The 4-Scale canopy model was used to model leaf reflectance for broadleaves and conifer needles using a-priori determined structural parameters (Table 3) over a range of different solar and viewing geometries $\vartheta_i = 29°–55°$; $\vartheta_r = 0°–33°$). The same model parameters and algorithm was performed for CASI, Landsat and MERIS derived reflectance factors. Fig. 5 displays measured (ground) leaf reflectance,

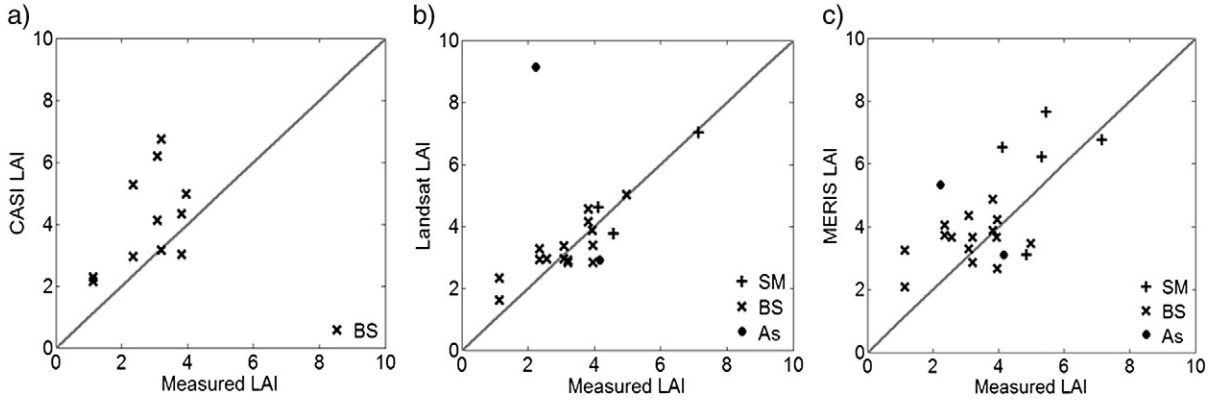

Fig. 4. Measured LAI against modelled LAI for a) CASI (RMSE = 1.82); b) Landsat 5 TM (RMSE = 1.67); c) MERIS (RMSE = 1.41). The 1:1 line is shown for all cases.

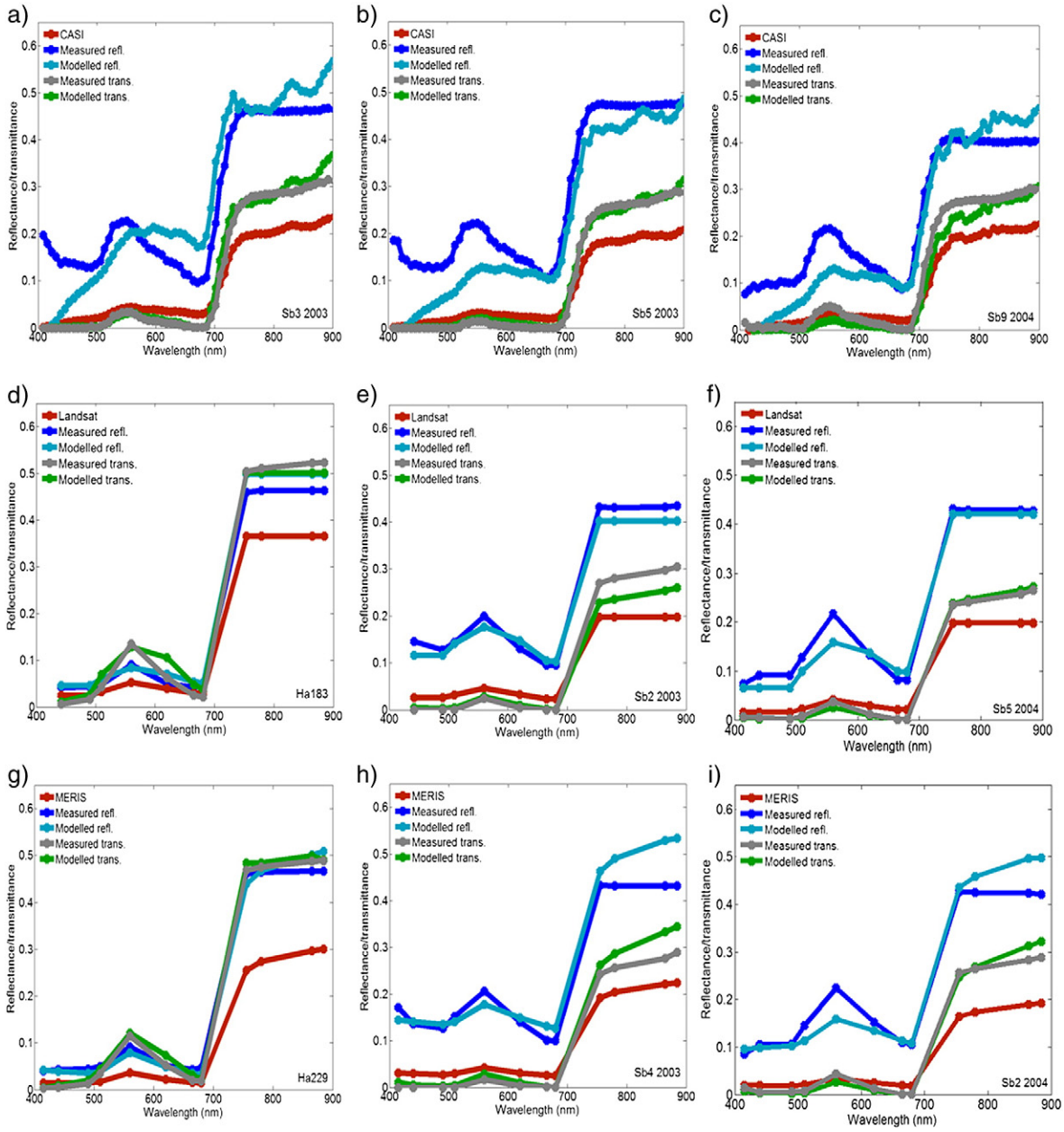

Fig. 5. Modelled and measured leaf reflectance and transmittance spectra and canopy reflectance for CASI, Landsat and MERIS data for broadleaf and coniferous sites.

modelled leaf reflectance from CASI, Landsat and MERIS pixels of three ground sites, and the original airborne or satellite reflectance spectra. The Landsat reflectance spectra contain modelled reflectance factors at MERIS wavelengths (see Section 2.2.4). The airborne or satellite reflectance spectra may not necessarily be the same for both sensors due to different acquisition conditions. Importantly, Fig. 5 demonstrates the correspondence between modelled and measured leaf reflectance spectra.

The leaf spectra are well modelled for Haliburton sites (Fig. 5d,g), which exhibit higher LAI values, closed canopies and less spatial heterogeneity than coniferous sites. Modelled results show a close correspondence with ground measurements for visible and near-infrared wavelengths, which are largely a function multiple scattering effects and is related to LAI and leaf distribution. The strong correlation between modelled and measured leaf spectra, for a range of image acquisition conditions, indicates that the model corrects well for varying solar and viewing geometries, which affects the relative contributions of sunlit and shaded foliage and background components. The CASI data contained low reflectance values below 500 nm due to problems with atmospheric correction in blue wavelengths. Reflectance factors from the two independent satellite data sources also demonstrate a consistency in modelled values. The accuracy of the leaf reflectance retrieval indicates that both the 4-Scale inversion algorithm and multiple scattering factor (Zhang et al., 2008a), are correcting for tree architecture and mutual shadowing within and between tree crowns. The LUT tables for deciduous and coniferous species are correctly parameterising forest structure and the manner in which leaf, branch and canopy structures interact with solar irradiance. The modelled leaf reflectance factors are now removed of canopy, background and image acquisition factors and can be used for leaf chlorophyll inversion.

3.2. Modelling foliar chlorophyll from ground measurements

In order to evaluate the accuracy of modelled leaf chlorophyll content from satellite reflectance data, it is first necessary to assess the inherent accuracy and uncertainty associated with the PROSPECT

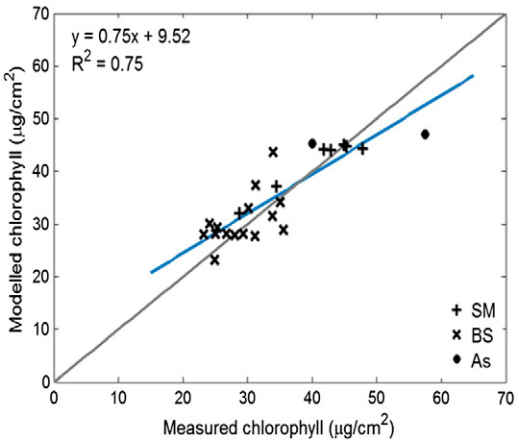

Fig. 6. Modelled leaf chlorophyll from PROSPECT against measured leaf chlorophyll for coniferous and broadleaf species ($p<0.001$; RSME = 4.28 µg/cm^2).

leaf radiative transfer model. Laboratory measured leaf chlorophyll content is compared to modelled leaf chlorophyll content derived from leaf reflectance factors measured using a spectroradiometer (Fig. 6), for both broadleaves and needles. The leaf area measured by the spectroradiometer directly corresponded to the area used to measure chlorophyll content in the laboratory. Only leaf reflectance at MERIS wavebands was used as an input into the PROSECT model. Consequently, this analysis removes any error associated with atmospheric scattering, spatial heterogeneity within a pixel and the influence of non-photosynthetic elements, background vegetation and changing LAI, to give a quantifiable indication of the accuracy of the leaf chlorophyll inversion model.

The strong relationship between measured and modelled leaf chlorophyll content exists despite the inclusion of different leaf shapes and internal structures and displays a high degree of linearity (slope = 0.75, intercept = 9.52). The strength of the regression (R^2 = 0.75) also compares well to previous findings, where Zarco-Tejada et al. (2004) found a relationship between needle leaf reflectance spectra and PROPSECT inverted chlorophyll content of $R^2 = 0.4$. Moorthy et al. (2008) found that comparisons between PROSPECT estimated needle-level pigment content and laboratory measurements yielded a RMSE of 12.6 µg/cm^2 with a $R^2 = 0.54$, which increased to yield an RMSE of 7.9 µg/cm^2, with the inclusion of a transmission normalization factor to account for the shape of conifer needles compared to broadleaves. Given the inclusion of both broadleaf and conifer needles spectra in the PROSPECT inversion, the dynamic range of chlorophyll content is large. The high coefficient of determination demonstrates the suitability of the leaf radiative transfer model for modelling leaf level chlorophyll for multiple species and leaf structures and shapes.

3.3. Modelling foliar chlorophyll content from airborne and satellite measurements

At the canopy scale, reflectance factors are a function of leaves, stems, branches and other non-photosynthetic materials, background material and shaded components. Consequently, it is important to account for these variables in deriving leaf reflectance from airborne or satellite platforms. The results for modelled leaf chlorophyll content from both Landsat and MERIS reflectance data are shown in Fig. 7. CASI (30 m) and Landsat chlorophyll results were produced from average modelled chlorophyll data from 3×3 pixels around the ground site to reduce the impacts of geographic location inaccuracies and the impact of non-vegetative influences on pixel reflectance, particularly as some of the sites were located close to roads which affected reflectance factors.

Both sources of satellite data show reasonably strong validation results ($R^2 = 0.65$ and 0.62, for Landsat and MERIS data, respectively), with a high linearity around the 1:1 line and a consistency between the different data sources and spatial resolutions. The relationship between leaf chlorophyll estimation obtained through 4-Scale and PROSPECT obtained slope values close to 1 (1.34 and 0.91) and small intercepts (9.81 and 4.83). The modelled CASI chlorophyll estimates also show a strong relationship to measured chlorophyll values, with results around the 1:1 line. A lower regression coefficient ($R^2 = 0.41$) is found than from Landsat and MERIS data, which is likely attributable to the smaller range of values tested, and an absence of higher chlorophyll contents from broadleaf sites. Nonetheless, the strong linearity around the 1:1 line in the results of all products indicates that there was no systematic underestimation or overestimation of leaf chlorophyll content using this algorithm and site structural parameters.

3.4. Cross-validation of modelled leaf chlorophyll content from Landsat and MERIS data

To assess the effects of sub-pixel heterogeneity on coarse spatial scale MERIS derived chlorophyll measurements, Landsat derived leaf chlorophyll content was aggregated to MERIS (1200 m) pixels. Fig. 8a was calculated by taking the mean reflectance in each Landsat band within each 1200 m MERIS pixel and applying the leaf reflectance inversion and leaf chlorophyll algorithm to the 1200 m reflectance. This aggregation method produced lumped leaf chlorophyll content (Chl_L) estimates. Fig. 8a compares leaf chlorophyll content retrieved from MERIS reflectance

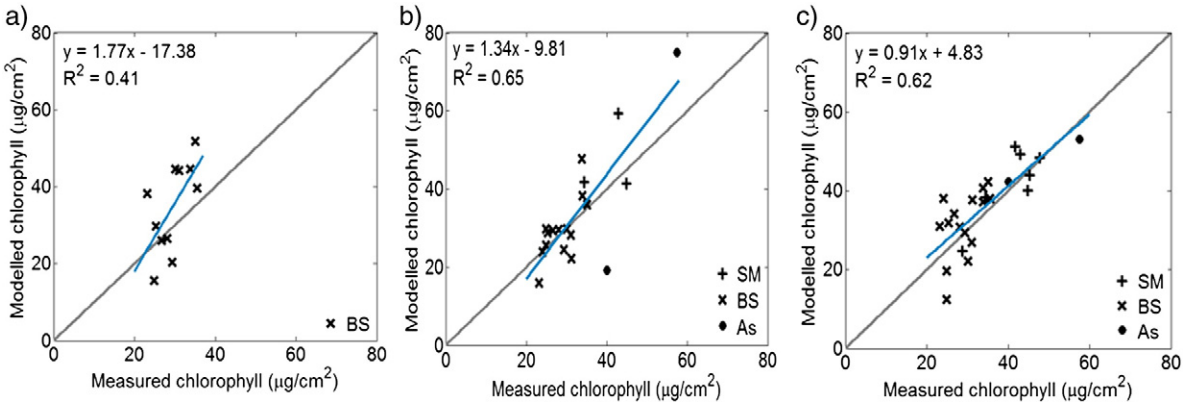

Fig. 7. Modelled and measured leaf chlorophyll content for a) CASI ($p<0.05$; 10.45 µg/cm^2); b) Landsat 5 Tm ($p<0.001$; 8.87 µg/cm^2) and c) MERIS ($p<0.001$; RSME = 6.42 µg/cm^2) data.

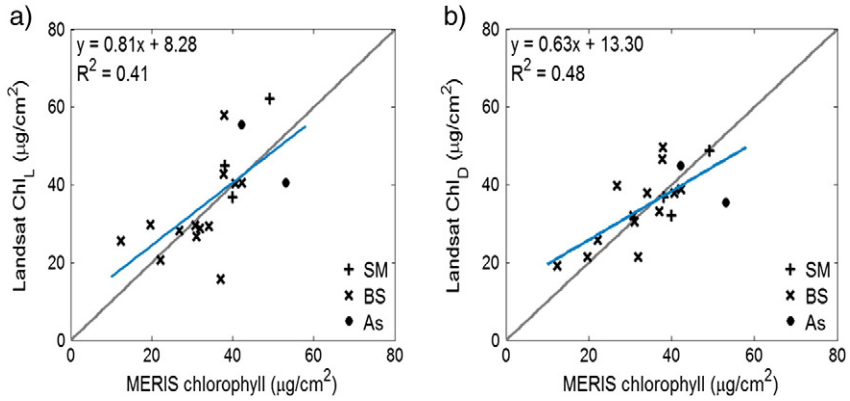

Fig. 8. The relationship between MERIS derived leaf chlorophyll content and scaled Landsat chlorophyll content a) Landsat lumped chlorophyll (Chl_L) values ($p<0.005$; RMSE = 9.93 μg/cm^2) and b) Landsat distributed chlorophyll (Chl_D) values ($p<0.01$; RMSE = 7.42 μg/cm^2).

and from aggregated Landsat reflectance at a 1200 m resolution (Chl_L). The relationship between the leaf chlorophyll content derived from the two sensors is highly significant ($p<0.005$).

As the relationships between surface reflectance in the various bands and the leaf chlorophyll are non-linear, it is expected that considerable error exists in the retrieved leaf chlorophyll content for the large 1200 m pixels when they are spatially heterogeneous. A more accurate way is to model leaf chlorophyll content at Landsat 30 m resolution and then aggregate the chlorophyll estimates to 1200 m resolution, giving distributed chlorophyll estimates (Chl_D) (Chen et al., 2002). This is because lumped (Chl_L) reflectance averaging process masks sub-pixel variations and introduces biases when used to retrieve surface parameters, even using the same algorithms (Chen, 1999). This is due to spatial differences in land cover, which causes non-linearity in the relationship between reflectance and leaf chlorophyll content. Fig. 8b shows the comparison of leaf chlorophyll content (Chl_D) calculated at 30 m resolution and scaled to 1200 m with leaf chlorophyll estimated from MERIS 1200 m reflectance data. The relationship exhibits a similar degree of scatter to Fig. 8a, and it is still around the 1:1 line, with a good linearity and statistical significance ($p<0.01$). Fig. 8b is more useful than Fig. 8a in assessing the accuracy of MERIS chlorophyll estimates because the Landsat results shown in Fig. 8b can remove much of the influence of surface heterogeneity on the chlorophyll content retrieval, while this influence remains in MERIS results. Further analysis is required to assess if the scatter around the 1:1 line in Fig. 8b could be attributed to surface heterogeneity with the 1200 m spatial extent.

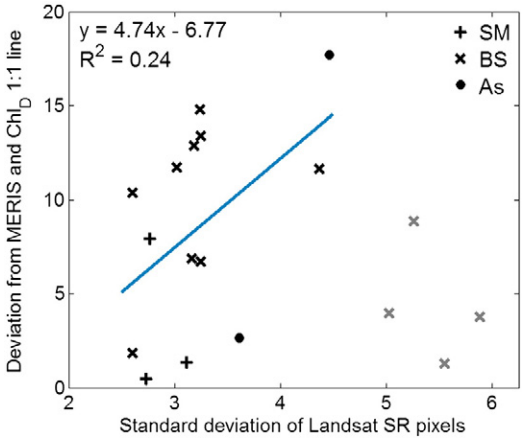

Fig. 9. Deviation from the 1:1 line between MERIS chlorophyll estimates and Landsat Chl_D against the standard deviation of Landsat SR pixel values ($p<0.01$).

3.5. Fine-scale spatial heterogeneity

Spatial heterogeneity in land cover and a nonlinearity of algorithms and their dependence on land cover types introduces uncertainties in coarse scale analysis (Chen, 1999; Ehleringer & Field, 1993; Simic et al., 2004). A textural approach was used to analyse the effects of Landsat and MERIS sub-pixel spatial heterogeneity and the scaling effect that occurs when moving from a fine spatial resolution to a coarser resolution (Hu & Islam, 1997). The simple ratio vegetation index (NIR/Red) was used to assess the spatial variability that existed within modelled Chl_D values (Bonan et al., 1993; Friedl, 1996). Fig. 9 shows the relationship between the standard deviation of SR values for Landsat Chl_D estimates against the distance of the Chl_D values from the 1:1 line with MERIS chlorophyll estimates (Fig. 8b).

Fig. 9 indicates that there is a weak relationship between sub-pixel heterogeneity (represented by the standard deviation of SR values) and differences found between Landsat Chl_D values and coarser scale MERIS chlorophyll estimates, covering the same spatial extent. Excluding four BS sites (in grey), differences in coarse-scale chlorophyll and Chl_D retrievals are related to the spatial variability within the MERIS pixel extent ($R^2 = 0.24$; $p<0.01$). The four excluded BS sites show large spatial variability (standard deviation > 5) but present a small numerical difference between modelled values from both products, indicating that spatial variability does not always lead to discrepancy in chlorophyll estimates. This suggests that both the type and composition of surface variables within a pixel contributes to scaling uncertainties.

3.6. Spatial variability in leaf chlorophyll content

The leaf chlorophyll content retrieval algorithm was applied over a broader, spatially continuous extent to investigate spatial variability in leaf chlorophyll distribution. The ability to produce such foliar chlorophyll maps provides a better understanding of temporal and spatial dynamics of chlorophyll variation. Spatially continuous maps are critical tools that can be used to monitor vegetation stress and remediation efforts, employ sustainable forest management practices and gain a better understanding of plant–environment interactions and the controlling mechanisms on chlorophyll content (Moorthy et al., 2008). Fig. 10 shows mapped leaf chlorophyll content for Sudbury 2003, using MERIS and Landsat data. Chlorophyll estimates are shown for a range of 0–100 μg/cm^2, due to the simulation of unrealistically high or low modelled results, particularly for water bodies.

The majority of leaf chlorophyll estimates appeared to range from 15 to 65 μg/cm^2, which is typical in young and mature needle leaf forest stands (Malenovský et al., 2006; Zarco-Tejada et al., 2004). Visual assessment of the mapped leaf chlorophyll estimates from Landsat and MERIS data show a high degree of spatial correlation (Fig. 10). The

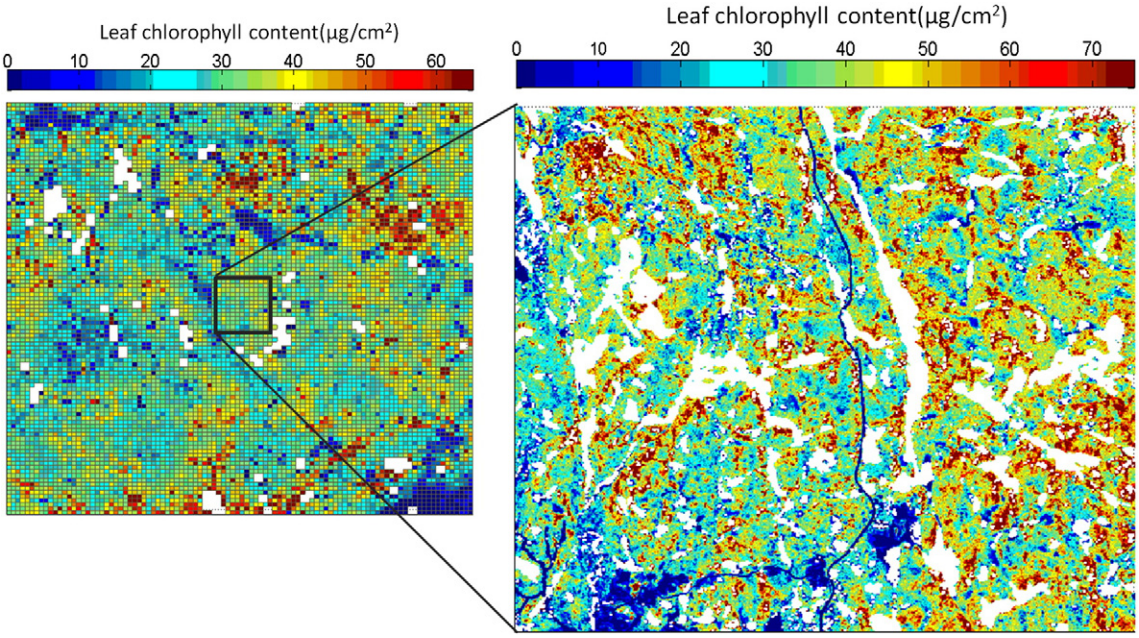

Fig. 10. Spatial variation in leaf chlorophyll content (μg/cm^2) for Sudbury (2003) from MERIS (1200 m) and Landsat TM (30 m) satellite data.

MERIS chlorophyll values are generally lower than those from Landsat, which is probably attributable to the spatial variation in leaf chlorophyll values that can be seen within the Landsat derived image. The presence of water bodies and bare ground, with zero or very low chlorophyll values has the effect of 'smoothing' out the coarser-scale estimates (Chl_D), removing the contribution of very high values. Lower MERIS estimates correspond to areas in the Landsat map representing both low leaf chlorophyll content and also water bodies, demonstrating the complexity associated with sub-pixel spatial heterogeneity. The spatial variability in pigment content could be attributed to environmental factors such as soil nutrient content, soil moisture content and slope, in addition to leaf age and stress. The MERIS chlorophyll map reveals coarser patterns of spatial variability which could be linked to local topography, associated soil moisture differences or exposure to light. The finer-scale Landsat map reveals the degree of localised spatial variation in leaf chlorophyll across the landscape, with localised patches of high values of chlorophyll (i.e. >70 μg/cm^2), within regions of already high chlorophyll estimates of 50 μg/cm^2. The areas displaying lower leaf chlorophyll contents (i.e. 20–30 μg/cm^2) in contrast are much broader and less in localised patches.

4. Conclusion

This research provides a theoretical basis for the future retrieval of spatially distributed leaf chlorophyll content over different spatial and temporal scales. Through the use of physically-based models, leaf level reflectance was retrieved from satellite-derived canopy reflectance, which was subsequently used to derive leaf chlorophyll estimates. In this paper we present several important developments and findings for obtaining leaf chlorophyll contents:

1. A physically-based approach, using a linked canopy model (4-Scale) and leaf radiative transfer model (PROSPECT), successfully accounted for differences in broadleaf and needle leaf structures and canopy architecture, producing a modelled leaf chlorophyll content result of $R^2 = 0.62$ ($p < 0.0001$) from MERIS satellite-derived reflectance data.
2. This modelled approach negates a site-specific dependency in the relationship between reflectance and leaf chlorophyll, and can potentially be accurately applied over a range of spatial extents and time frames without explicitly requiring ground calibration.
3. Leaf chlorophyll estimates showed consistent validation results using two independent data sources (MERIS and Landsat 5 TM), and at two different spatial resolutions (1200 m and 30 m, respectively). Landsat and MERIS satellite data resulted in a good relationship between ground measured values and modelled estimates ($R^2 = 0.65$ and 0.62, respectively), and a strong linearity.
4. The spatial heterogeneity that may exist within a coarse pixel size (1200 m) can lead to a degree of uncertainty in modelled leaf chlorophyll. Although results suggest a lack of systematic bias, contributions from non-vegetated elements such as water bodies and areas of bare ground can result in greater scattering and a weaker relationship.

The results presented in this paper compare favourably to other studies, e.g. (Moorthy et al., 2008; Zarco-Tejada et al., 2004; Zhang et al., 2008a), particularly as previous research has often been restricted to a single vegetation type or species. The application of this algorithm at broad spatial extents enables the production of foliar chlorophyll maps, which are powerful tools for promoting a better understanding of chlorophyll dynamics over space and time. Spatially continuous maps are vital for monitoring vegetation stress and for enhancing understanding of plant-environment interactions and the controlling mechanisms on chlorophyll content (Moorthy et al., 2008). The ability of this technique to characterise variations in chlorophyll content across different vegetation species and canopy structures is important for making the method operational across coarser spatial extents, and for its inclusion in photosynthesis and carbon cycle models.

References

Abuelgasim, A. A., Fernandes, R. A., & Leblanc, S. G. (2006). Evaluation of National and Global LAI products derived from optical remote sensing instruments over Canada. *IEEE Transactions on Geoscience and Remote Sensing*, *44*(7), 1872–1884.

Asner, G. P., & Martin, R. E. (2008). Spectral and chemical analysis of tropical forests, Scaling from leaf to canopy levels. *Remote Sensing of Environment*, *112*, 3958–3970.

Berk, A., Bernstein, L. S., Anderson, G. P., Acharya, P. K., Robertson, D. C., Chetwynd, J. H., et al. (1998). MODTRAN cloud and multiple scattering upgrades with application to AVIRIS. *Remote Sensing of Environment*, *65*, 367–375.

Blackburn, G. A. (1998). Quantifying chlorophylls and carotenoids at leaf and canopy scales, An evaluation of some hyperspectral approaches. *Remote Sensing of Environment*, *66*, 273–285.

Bonan, G. B., Pollard, D., & Thomson, S. L. (1993). Influence of subgridscale heterogeneity in leaf area index, stomatal resistance, and soil moisture on grid-scale land–atmosphere interactions. *Journal of Climate*, *6*, 1882–1896.

Broge, N. H., & Leblanc, E. (2001). Comparing prediction power and stability of broadband and hyperspectral vegetation indices for estimation of green leaf area index and canopy chlorophyll density. *Remote Sensing of Environment*, *76*(2), 156–172.

Canisius, F., Fernandes, R., & Chen, J. M. (2010). Comparison and evaluation of medium resolution imaging spectrometer leaf area index products across a range of land use. *Remote Sensing of Environment*, *114*, 950–960.

Caspersen, J. P., & Saprunoff, M. (2005). Seedling recruitment in a northern temperate forest, the relative importance of supply and establishment limitation. *Canadian Journal of Forest Research*, *35*, 978–989.

Chander, G., Markham, B. L., & Helder, D. L. (2009). Summary of current radiometric calibration coefficients for Landsat MSS, TM, ETM+, and EO-1 ALI sensors. *Remote Sensing of Environment*, *113*, 893–903.

Chavez, P. S. (1988). An improved dark-object subtraction technique for atmospheric scattering correction of multispectral data. *Remote Sensing of Environment*, *24*, 459–479.

Chavez, P. S. (1996). Image-based atmospheric corrections — Revisited and Improved. *Photogrammetric Engineering and Remote Sensing*, *62*(9), 1025–1036.

Chen, J. M. (1999). Spatial scaling of a remote sensed surface parameter by contexture. *Remote Sensing of Environment*, *69*, 30–42.

Chen, J. M., & Cihlar, J. (1995). Plant canopy gap size analysis theory for improving optical measurements of leaf area index. *Applied Optics*, *34*, 6211–6222.

Chen, J. M., & Cihlar, J. (1996). Retrieving leaf area index of boreal conifer forests using Landsat TM images. *Remote Sensing of Environment*, *55*, 153–162.

Chen, J. M., & Leblanc, S. (1997). A 4-scale bidirectional reflection model based on canopy architecture. *IEEE Transactions on Geoscience and Remote Sensing*, *35*, 1316–1337.

Chen, J. M., & Leblanc, S. G. (2001). Multiple-scattering scheme useful for hyperspectral geometrical optical modelling. *IEEE Transactions on Geoscience and Remote Sensing*, *39*(5), 1061–1071.

Chen, J. M., Pavlic, G., Brown, L., Cihlar, J., Leblanc, S. G., White, H. P., et al. (2002). Validation of Canada-wide leaf area index maps using ground measurements and high and moderate resolution satellite imagery. *Remote Sensing of Environment*, *80*, 165–184.

Chen, J. M., Rich, P. M., Gower, T. S., Norman, J. M., & Plummer, S. (1997). Leaf area index of boreal forests, theory, techniques and measurements. *Journal of Geophysical Research*, *102*, 29,429–29,444.

Curran, P. J., Dungan, J. L., & Gholz, H. L. (1990). Exploring the relationship between reflectance red edge and chlorophyll content in slash pine. *Tree Physiology*, *7*, 33–48.

Curran, P. J., & Steele, C. M. (2005). MERIS, The rebranding of an ocean sensor. *International Journal of Remote Sensing*, *26*, 1781–1798.

Daughtry, C. S. T., Walthall, C. L., Kim, M. S., de Colstoun, E. B., & McMurtrey, J. E. (2000). Estimating corn leaf chlorophyll concentration from leaf and canopy reflectance. *Remote Sensing of Environment*, *74*, 229–239.

Dawson, T. P., Curran, P. J., & Plummer, S. E. (1998). LIBERTY — Modeling the effects of leaf biochemical concentration on reflectance spectra. *Remote Sensing of Environment*, *65*(1), 50–60.

Demarez, V., & Gastellu-Etchegorry, J. P. (2000). A modeling approach for studying forest chlorophyll content. *Remote Sensing of Environment*, *71*, 226–238.

Ehleringer, J. R., & Field, C. B. (1993). *Scaling physiological processes, Leaf to globe*. Boston: Academic.

Fisher, J. I., & Mustard, J. F. (2007). Cross-scalar satellite phenology from ground, Landsat, and MODIS data. *Remote Sensing of Environment*, *109*, 261–273.

Friedl, M. A. (1996). Examining the effects of sensor resolution and subpixel heterogeneity on spectral vegetation indices, Implications for biophysical modeling. In D. A. Quattrochi, & M. F. Goodchild (Eds.), *Scaling of remote sensing data for GIS* (pp. 113–139). New York: Lewis Publishers.

Gamon, J. A., & Surfus, J. S. (1999). Assessing leaf pigment content and activity with a reflectometer. *New Phytologist*, *143*, 105–117.

Gastellu-Etchegorry, J. P., Demarez, V., Pinel, V., & Zagolski, F. (1996). Modelling radiative transfer in heterogeneous 3-D vegetation canopies. *Remote Sensing of Environment*, *58*, 131–156.

Gitelson, A. A., Gritz, Y., & Merzlyak, M. N. (2003). Relationships between leaf chlorophyll content and spectral reflectance and algorithms for non-destructive chlorophyll assessment in higher plant leaves. *Journal of Plant Physiology*, *160*, 271–282.

Gitelson, A. A., Viña, A., Verma, S. B., Rundquist, D. C., Arkebauer, T. J., Keydan, G., et al. (2006). Relationship between gross primary production and chlorophyll content in crops, Implications for the synoptic monitoring of vegetation productivity. *Journal of Geophysical Research D, Atmospheres*, *111*.

Goel, N. S., & Thompson, R. L. (2000). A snapshot of canopy reflectance models and a universal model for the radiation regime. *Remote Sensing Reviews*, *18*, 197–225.

Goodenough, D., Li, J., Asner, G., Schaepman, M., Ustin, S., & Dyk, A. (2006). Combining hyperspectral remote sensing and physical modelling for applications in land ecosystems. *IEEE International Geoscience and Remote Sensing Symposium (IGARSS). 2000–2004*.

Gradowski, T., & Thomas, S. C. (2006). Phosphorus limitation of sugar maple growth in central Ontario. *Forest Ecology and Management*, *226*(1–3), 104–109.

Guyot, G., & Gu, X. F. (1994). Effect of radiometric corrections on NDVI determined from SPOT HRV and Landsat TM data. *Remote Sensing of Environment*, *49*, 169–180.

Harron, J. W. (2000, December). *Optical properties of phytoelements in conifers*. MSc Thesis. Graduate Program in Earth and Space Science (pp. 193). Toronto: York University.

Harron, J. W., & Miller, J. R. (1995). An alternative methodology for reflectance and transmittance measurements of conifer needles. *17th Canadian Symposium on Remote Sensing, Saskatoon, Saskatchewan, II* (pp. 654–661). Ottawa, Canada: Canadian Remote Sensing Society, Canadian Aeronautics and Space Institute.

Hu, Z., & Islam, S. (1997). A framework for analyzing and designing scale invariant remote sensing algorithm. *IEEE Transactions on Geoscience and Remote Sensing*, *35*, 747–755.

Inoue, Y. (2003). Synergy of remote sensing and modeling for estimating ecophysiological processes in plant production. *Plant Production Science*, *6*, 3–16.

Jacquemoud, S., Bacour, C., Poilve, H., & Frangi, J. P. (2000). Comparison of four radiative transfer models to simulate plant canopies reflectance, direct and inverse mode. *Remote Sensing of Environment*, *74*, 471–481.

Jacquemoud, S., & Baret, F. (1990). PROSPECT, a model of leaf optical properties spectra. *Remote Sensing of Environment*, *34*, 75–91.

Jacquemoud, S., Baret, F., Andrieu, B., Danson, F. M., & Jaggard, K. (1995a). Extraction of vegetation biophysical parameters by inversion of the PROSPECT + SAIL models on sugar beet canopy reflectance data—Application to TM and AVIRIS sensors. *Remote Sensing of Environment*, *52*, 163–172.

Jacquemoud, S., Verdebout, J., Schmück, G., Andreoli, G., & Hosgood, B. (1995b). Investigation of leaf biochemistry by statistics. *Remote Sensing of Environment*, *54*(3), 180–188.

Jacquemoud, S., Verhoef, W., Baret, F., Bacour, C., Zarco-Tejada, P. J., Asner, G. P., et al. (2009). PROSPECT + SAIL models, A review of use for vegetation characterization. *Remote Sensing of Environment*, *113*(1), S56–S166.

Jenkins, J. P., Braswell, B. H., Frolking, S. E., & Aber, J. D. (2002). Detecting and predicting spatial and interannual patterns of temperate forest springtime phenology in the eastern U.S. *Geophysical Research Letters*, *29*, 54.

Kötz, B., Morsdorf, F., Itten, K., Schaepman, M., Bowyer, P., & Allgöwer, B. (2004). Radiative transfer modeling within a heterogeneous canopy for estimation of forest fire fuel properties. *Remote Sensing of Environment*, *92*, 332–344.

Kurcharik, C. J., Norman, J. M., Murdock, L. M., & Gower, S. T. (1997). Characterizing canopy nonrandomness with a multiband vegetation imager (MVI). *Journal of Geophysical Research*, *102*(D24), 29 455–29 473.

Kuusk, A. (1985). The hot spot effect of a uniform vegetative cover. *Soviet Journal of Remote Sensing*, *3*, 645–658.

Le Maire, G., François, C., & Dufrêne, E. (2004). Towards universal broad leaf chlorophyll indices using PROSPECT simulated database and hyperspectral reflectance measurements. *Remote Sensing of Environment*, *89*, 1–28.

Leithead, M., Anand, M., Duarte, L., & Pillar, V. D. (2012). Causal effects of latitude, disturbance and dispersal limitation on richness in a recovering temperate, subtropical and tropical forest. *Journal of Vegetation Science*, *23*, 339–351.

Li, X., Strahler, A. H., & Woodcock, C. E. (1995). A hybrid geometric optical-radiative transfer approach to modeling albedo and directional reflectance of discontinuous canopies. *IEEE Transactions on Geoscience and Remote Sensing*, *33*, 466–480.

Mahiny, A. S., & Turner, B. J. (2007). A comparison of four common atmospheric correction methods. *Photogrammetric Engineering and Remote Sensing*, *73*, 361–368.

Malenovský, Z., Albrechtová, J., Lhotáková, Z., Zurita-Milla, R., Clevers, J. G. P. W., Schaepman, M. E., et al. (2006). Applicability of the PROSPECT model for Norway spruce needles. *International Journal of Remote Sensing*, *27*(24), 5315–5340.

Markham, B. L., & Barker, J. L. (1986). *Landsat MSS and TM post-calibration dynamic ranges, exoatmospheric reflectances and at-satellite temperatures*. EOSAT Technical Notes.

Merzlyak, M. N., & Gitelson, A. A. (1995). Why and what for the leaves are yellow in autumn? On the interpretation of optical spectra of senescing leaves (Acer platanoides L.). *Journal of Plant Physiology*, *145*, 315–320.

Moorthy, I., Miller, J. R., & Noland, T. L. (2008). Estimating chlorophyll concentration in conifer needles with hyperspectral data, an assessment at the needle and canopy level. *Remote Sensing of Environment*, *112*, 2824–2838.

O' Neill, N. T., Zagolski, F., Bergeron, M., Royer, A., Miller, J. R., & Freemantle, J. (1997). Atmospheric correction validation of CASI images acquired over the BOREAS southern study area. *Canadian Journal of Remote Sensing*, *23*, 143–162.

Rayfield, B., Anand, M., & Laurence, S. (2005). Assessing simple versus complex restoration strategies for industrially disturbed forests. *Restoration Ecology*, *13*(4), 639–650.

Richardson, A. D., Duigan, S. P., & Berlyn, G. P. (2002). An evaluation of non-invasive methods to estimate foliar chlorophyll content. *New Phytologist*, *153*, 185–194.

Rowe, J. S. (1972). *Forest regions of Canada. Publication 1 300*. Ottawa: Department of the Environment, Canadian Forestry Service (172 pp.).

Sampson, P. H., Zarco-Tejada, P. J., Mohammed, G. H., Miller, J. R., & Noland, T. L. (2003). Hyperspectral remote sensing of forest condition, Estimating chlorophyll content in tolerant hardwoods. *Forest Science*, *49*, 381–391.

Sharma, A. R., Badarinath, K. V. S., & Roy, P. S. (2009). Comparison of ground reflectance measurement with satellite derived atmospherically corrected reflectance, A case study over semi-arid landscape. *Advances in Space Research*, *43*(1), 56–64.

Simic, A., Chen, J. M., Freemantle, J. R., Miller, J. R., & Pisek, J. (2010). Improving clumping and lai algorithms based on multiangle airborne imagery and ground measurements. *IEEE Transactions on Geoscience and Remote Sensing*, *48*, 1742–1759.

Simic, A., Chen, J. M., Liu, J., & Csillag, F. (2004). Spatial scaling of net primary productivity using subpixel information. *Remote Sensing of Environment*, *93*, 246–258.

Simic, A., Chen, J. M., & Noland, T. L. (2011). Retrieval of forest chlorophyll content using canopy structure parameters derived from multi-angle data, the measurement concept of combining nadir hyperspectral and off-nadir multispectral data. *International Journal of Remote Sensing*, *32*(20), 5621–5644.

Sims, D. A., & Gamon, J. A. (2002). Relationship between leaf pigment content and spectral reflectance across a wide range species, leaf structures and development stages. *Remote Sensing of Environment*, *81*, 337–354.

Steven, M. D., Malthus, T. J., Baret, F., Xu, H., & Chopping, M. J. (2003). Intercalibration of vegetation indices from different sensor systems. *Remote Sensing of Environment*, *88*(4), 412–422.

Ustin, S. L., Roberts, D. A., Gamon, J. A., Asner, G. P., & Green, R. O. (2004). Using imaging spectroscopy to study ecosystem processes and properties. *Bioscience*, *54*, 523–534.

Verhoef, W. (1984). Light scattering by leaf layers with application to canopy reflectance modeling, The SAIL model. *Remote Sensing of Environment*, *16*, 125–141.

Vermote, E. F., Tanre, D., Deuze, J. L., Herman, M., & Morcrett, J. J. (1997). Second simulation of the satellite signal in the solar spectrum, 6S, an overview. *IEEE Transactions on Geoscience and Remote Sensing*, *35*, 675–686.

Verrelst, J., Schaepman, M. E., Malenovský, Z., & Clevers, J. G. P. W. (2010). Effects of woody elements on simulated canopy reflectance, Implications for forest chlorophyll content retrieval. *Remote Sensing of Environment*, *114*, 647–656.

Weiss, M., Baret, F., Garrigues, S., & Lacaze, R. (2007). LAI and fAPAR CYCLOPES global products derived from VEGETATION. Part 2, Validation and interõcomparison with MODIS Collection 4 products. *Remote Sensing of Environment*, *110*(3), 317–331.

Zarco-Tejada, P. J., Miller, J. R., Harron, J., Hu, B., Noland, T. L., Goel, N., et al. (2004). Needle chlorophyll content estimation through model inversion using hyperspectral data from boreal conifer forest canopies. *Remote Sensing of Environment*, *89*, 189–199.

Zarco-Tejada, P. J., Miller, J. R., Mohammed, G. H., Noland, T. L., & Sampson, P. H. (2002). Vegetation stress detection through chlorophyll a + b estimation and fluorescence effects on hyperspectral imagery. *Journal of Environmental Quality*, *31*, 1433–1441.

Zarco-Tejada, P. J., Miller, J. R., Noland, T. L., Mohammed, G. H., & Sampson, P. H. (2001). Scaling-up and model inversion methods with narrowband optical indices for chlorophyll content estimation in closed forest canopies with hyperspectral data. *IEEE Transactions on Geoscience and Remote Sensing*, *39*, 1491–1507.

Zhang, Y. (2011). Forest leaf chlorophyll content study using hyperspectral remote sensing. In P. S. Thenkabail, J. G. Lyon, & A. Huete (Eds.), *Hyperspectral Remote Sensing of Vegetation* (pp. 167–186). CRC Press.

Zhang, Y., Chen, J. M., Miller, J. R., & Noland, T. L. (2008a). Leaf chlorophyll content retrieval from airborne hyperspectral remote sensing imagery. *Remote Sensing of Environment*, *112*, 3234–3247.

Zhang, Y., Chen, J. M., Miller, J. R., & Noland, T. L. (2008b). Retrieving chlorophyll content of conifer needles from hyperspectral measurements. *Canadian Journal of Remote Sensing*, *34*(3), 296–310.

Zhang, Y., Chen, J. M., & Thomas, S. C. (2007). Retrieving seasonal variation in chlorophyll content of overstorey and understorey sugar maple leaves from leaf-level hyperspectral data. *Canadian Journal of Remote Sensing*, *5*, 406–415.